AERODYNAMICS OF V/STOL AIRCRAFT POWERED BY LIFT FANS

By David H. Hickey* and Woodrow L. Cook**

SUMMARY

Data from investigations in the Ames Research Center's 40- by 80-Foot Wind Tunnel of large-scale V/STOL models powered with lift fans are presented and analyzed to show the important parameters affecting induced lift, drag, and pitching moment. While these effects can sometimes be accurately calculated for fan-in-wing installations, a better understanding of the limitations of the calculations is required to allow confident predictions. It is shown that the downwash from lifting fans or engines mounted upstream of a wing unload the wing during transition. Lift-fan powered VTOL aircraft are shown to have significant overload STOL capability if a gas power transfer control system is used, but with a separate control system the overload capability may be small. Finally, it is shown that boundary-layer control can provide good inlet performance for very thin fan installations that have small inlet radii.

*Research Scientist, Ames Research Center, NASA, Moffett Field, California 94035.

**Acting Assistant Division Chief, Full-Scale and Systems Research Division, Ames Research Center, NASA, Moffett Field, California 94035.

1. INTRODUCTION

NASA Ames Research Center is conducting a comprehensive experimental research program with large-scale V/STOL models powered with lift fans to define the aerodynamic characteristics of fan powered aircraft in transition. Aerodynamic interference between the fans and the airframe, transition performance, stability and control, and installation problems are being studied. Configurations examined thus far include single and multiple fan-in-wing arrangements, remote fuselage-mounted fans, and tandem fans (1-6).

This paper will summarize these experimental results and discuss the calculation of some of the more important characteristics. Specifically, the topics to be covered are induced lift, drag, moment variation with airspeed, trailing-edge flap contributions, ground effect in hover, transition performance, and the application of boundary-layer control to lift-fan inlets.

2. DESCRIPTION OF MODELS

Photographs of two typical lift-fan powered models installed in the 40- by 80-foot wind tunnel are shown in Fig. 1. All model configurations tested and some of their pertinent dimensions are listed in Table 1. When the models had more than one pair of symmetrical fans (models 4, 6, and 7), several fan arrangements were tested; these are identified by a model number and letter. Wing span of the models varied from approximately 30 to 40 feet. Wing area varied from 230 to 426 square feet. Model 1 (1,2) featured an inlet one diameter deep with a circular inlet vane. Models 2 (3) and 3 (4) are typical fan-in-wing configurations; model 3 was intended to represent the Ryan XV-5A. Model 4 not only has a spanwise variation of fans, but the 4 inboard fans could be varied chordwise. Model 5 has a 6-percent-thick delta wing. In order to permit fan installation in this small depth, it was necessary to modify the fan (discussed later) and provide blowing boundary-layer control on the very small fan radius available in the outer half of the wing. Model 6 (5,6) has tandem fans as well as the fans mounted at the extremities of the wing chord. Model 7 (5,6) has remote fans mounted on the fuselage; the forward lift fan could be mounted at several places and the rear fan is a rotating lift-cruise fan.

2.1 Power Plants

General Electric tip turbine driven lift fans were used in all the models. Models 1, 2, 3, and 5 had 5.2-foot-diameter fans similar to the wing fans in the Ryan XV-5A. Models 4, 6, and 7 had 3-foot-diameter fans similar to the XV-5A pitch fan. Both fan types were designed to have about 1.1 pressure ratio. The fans of all models except number 5 consisted of an inlet, rotor, and downstream stator. The downstream

stator was removed from model 5 so that the fan could be installed in the 5-percent-thick delta wing. The outer 180° of the lift-fan inlet was fitted with a slot to provide blowing boundary-layer control on the very small inlet radius (radius to diameter ratio as small as 0.016).

Inlet configuration and performance of the models varied markedly: for model 1 (deep inlet with circular vane) the inlet provided nearly theoretical thrust variation with airspeed (full ram recovery) over the transition speed range; for models 2, 3, 5, 6, and 7 (shallow inlets typical of fan-in-wing installations) the thrust increased at very low speeds and dropped to 80 to 90 percent of the zero airspeed thrust at the high speed end of transition; for model 4 with all six fans operating, thrust at forward speed was always less than the zero airspeed value (in one case, 60 percent). All fans except the rotating cruise fan (model 7) had a cascade of exit louvers similar to those used on the Ryan XV-5A to vector fan thrust for horizontal force in the transition flight regime.

One J-85 engine powered one 5.2-foot-diameter fan or four 3-foot-diameter fans. When models 4, 6, and 7 were [illegible] with two or six fans, the excess J-85 flow was exhausted exter[illegible] these cases, model forces and moments were corrected for the e[illegible] excess flow.

2.2 Model Sizing

From comparison of wind-tunnel and flight-test results, ratios have been derived (7) of model-to-wind-tunnel size that are known to give negligibly small wall effects. Fig. 2 shows the relative size of the models investigated with respect to the recommended boundaries. The ratio of fan area (lifting element area) to wind-tunnel cross-sectional area was within prescribed limits for all models. However, momentum-area ratios and span-to-tunnel width ratios were, in most cases, larger than the recommended values. The recommended boundaries (7) are based on limited experience and represent tentative boundaries based on limited data. More experience may indicate the feasibility of increasing model sizes. Furthermore, for aircraft that have concentrated lifting elements, such as lift fans, the most important parameter is probably the area ratio of the lifting element. Based on this reasoning, the wind-tunnel wall effects are believed to be small, and the results are uncorrected.

3. RESULTS AND DISCUSSION

This section of the paper is organized in three parts. The first part deals with the interference between the fan airflows and the aircraft flow field, and the effect of this interference on lift, drag, and moment. The second part of the paper deals briefly with performance;

that is, hover ground effect and transition performance. The third part of the paper presents recent work with boundary-layer control applied to lift-fan inlets to permit very thin lift-fan installations.

3.1 Interference Effects

Drawing air from the upper side of a lifting surface and exhausting it at high velocity from the lower surface (as a fan-in-wing does) induces lift and moment on the wing, causes drag forces, and changes trailing-edge flap effectiveness. Fans operating outside the wing can also affect the flow field about the wing. The sense and magnitude of these forces depend on wing geometry, fan location in or about the wing, and relative size of the fan and wing.

3.1.1 Induced lift.- Figure 3 shows the variation of the ratio of total model lift to fan static thrust with flight speed ratio (that is, the ratio of free stream to fan exit airspeed). The absolute airspeed shown corresponds to that of fans with a pressure ratio of 1.3. The data show that the lift variation with forward speed can either be positive or negative, depending on fan location. With fans near the wing trailing edge, lift was increased more than 20 percent at 50 knots. The induced lift shown in Fig. 4 for the same models was obtained by subtracting fan thrust and power-off wing lift. A comparison of this figure with Fig. 3 shows that the large difference between the models in the variation of lift with forward speed is caused by different induced lift.

All other variables being equal, induced lift is an inverse function of fan area to wing area ratio (8). Fig. 5 shows the variation with the fan-to-wing area ratio of induced lift to static thrust ratio at a flight velocity ratio of 0.4. Of the 11 fan-in-wing configurations 6 fall in a narrow band; however, models 4 and 6 are strongly influenced by chordwise location. Induced lift increases as fans are moved aft. The figure also indicates that if several small fans are distributed spanwise, induced lift for a given fan area to wing area ratio will be higher than if a single large fan is placed near the wing root. To evaluate the effect of wing geometry, fan location, and fan distribution, without the effect of area ratio, the product of the ratio of induced lift to static thrust times the ratio of fan-to-wing area was calculated. Fig. 6 shows the variation of this value with flight velocity ratio for models 4 and 6. Again, the strong effect of fan chordwise position is shown, but without the effect of area ratio, induced lift of model 6b is less than that for model 4a, indicating that distributing the fans spanwise overcame the effect of chordwise location. Maximum induced lift would probably be given by a configuration that takes advantage of both effects, that is, fans distributed spanwise at the wing trailing edge.

3.1.2 Calculation of induced lift on fan-in-wing aircraft.- The effect on induced lift of the interrelationships between wing geometry, number of fans, fan location, and fan area to wing area ratio is complex. A comprehensive and reasonably accurate theoretical approach is required for predicting both lift and moment. None of the theoretical approaches published to date have shown good agreement with theory for the many possible fan-in-wing arrangements. One simplified approach uses two-dimensional jet flap theory and three-dimensional wing theory (8). The flow model postulated is shown in Fig. 7. The equation for induced lift (8) can be expressed as

$$\frac{\Delta L_i}{T_s} = \frac{V_o^2}{V_{j_s}^2} \frac{C_{L_{\delta_1}}}{4\pi A_f/S} \left[\frac{C_l}{\delta_j} \cdot \delta_j \frac{S_1}{S_{2d}} + C_{l_3} \frac{S_3}{S_{2d}} \right] \qquad (1)$$

where $C_{L_{\delta_1}}$ is dependent on wing geometry and diameter to span ratio and the relationship in the brackets is the two-dimensional lift coefficient based on the total shaded area in Fig. 7. The gross wing area and aspect ratio of model 6 were used in the calculation. The two tandem fans (model 6a) were represented by a slot 1 diameter wide and 2 diameters long midway between the fans. In Fig. 8(a) the measured induced lift is compared to the induced lift calculated by the equation. In nearly all cases, induced lift was less than predicted.

One problem in the theoretical approach to the calculation of induced lift is defining the load-carrying ability of the portion of the wing aft of the fan because the flow is separated on the lower surface. This portion of the loading is represented by $C_{l_3}(S_3/S_{2d})$ in Eq. (1). The experimental results were analyzed to determine what other factor would produce better agreement between experiment and theory. Replacing C_{l_3} by $-(V_j/V)^{3/2}$ was found to improve agreement as shown in Fig. 8(b). The data for other velocity ratios are compared with the modified equation in Fig. 9. Although the agreement is good for many configurations, the equation does not adequately account for such fundamentals as the effect of spanwise distribution of fans on induced lift; therefore, improved theoretical approaches and a basic understanding of the phenomena involved are required.

3.1.3 Induced effects of fans mounted on a fuselage.- Unloading of the wing by downwash induced by a fan or engine is possible for fuselage mounted fans. Lift fans were tested in three locations in front of the wing on model 7. Fig. 10 presents the ratio of total lift-to-fan static thrust as a function of flight velocity ratio for these three front lift-fan locations. The low fan position just forward of the wing leading edge has the largest lift-to-thrust ratio over the whole velocity ratio range. Surprisingly, even if power-off wing lift is subtracted from the total, an increase of lift with forward speed is indicated rather than the expected reduction of lift due to fan induced wing download. In order to analyze

this result, wing lift was obtained from static pressure distributions and is shown in Fig. 11. The results indicate that in all locations fan operation did cause negative wing lift over part of the velocity ratio range, and, in the worst fan location, caused negative wing lift at all airspeeds.

The wing lift in Fig. 11 was subtracted from the total lift in Fig. 10 to give the total lift of the front fan; the upper shaded band in Fig. 12 shows this result as a function of airspeed. The lower band of data represents the fan thrust measured by a pressure survey of the fan wake. These bands represent the scatter in the data from the three configurations. Lift on the fan fairings, induced by fan operation, is indicated by the difference between the two sets of data. These results indicate that the lift induced on the front fan fairings by fan operation is large enough to overcome the download on the wing caused by downwash from the fan so that lift increases with airspeed.

The lift of model 7 with just the cruise fans operating is shown as a function of airspeed in Fig. 13 for two duct angles. The locus of the thrust equal to drag is also shown. For values when airplane drag is trimmed the total lift of the duct (wing lift subtracted from the data in Fig. 13) is greater than static thrust despite the trigonometric relationship between lift and thrust. This lift is a significant feature of ducted fan aerodynamics.

The variation of lift-to-thrust ratio with velocity ratio or airspeed (assuming a fan pressure ratio of 1.3) for a complete lift-cruise fan configuration for which the thrust has been vectored to balance the drag is shown in Fig. 14. The lines in the shaded area represent constant duct angle; the drag with a given duct angle was balanced at each airspeed by adjusting the lift-fan exit louver angle. The shaded area indicates the sensitivity of lift-to-thrust ratio to the combinations of duct and vector angles required to balance drag. These results show a marked increase in the lift ratio with flight velocity ratio which, at higher speeds, is due entirely to the trailing-edge flap. Apparently, at higher speeds downwash from the flap and front fans reduced the cruise fan effective angle of attack so that positive induced lift of the front and rear fans was cancelled.

The effective contribution to lift of a lift fan mounted in the nose of model 3 is shown in Fig. 15. Nose fan thrust actually increased with airspeed, but the downwash from the nose fan reduced overall model lift until, at a velocity ratio of 0.5, only 40 percent of the fan static thrust appeared as lift. Similar results are shown in Fig. 16 for model 4 with rotating jet engine nozzles mounted upstream of the wing. Since these results are for an engine with a hot exhaust, momentum ratio must be used as the independent variable rather than velocity ratio. The lift contribution of the engines was reduced by downwash from the engines acting on the wing, but the reduction was

much less than with the nose fan in model 3. These results indicate that fans or engines located upstream of the wing should be avoided, but if such a location is necessary, the lifting elements should be minimum size. Furthermore, the control system should be designed so that these elements can be shut down at the lowest practicable airspeed.

3.1.4 Drag in transition.- Computation of the drag caused by the turning of airflow into the fan (ram drag) has provided good estimates of the variation of drag with airspeed for some models (8). Results in Fig. 17 from model 4 indicate, however, that this result was fortuitous. The variation of ram drag to static thrust ratio with flight velocity ratio from the 2-, 4-, and 6-fan configurations falls in a small band, while the measured values for the 2-fan configuration are much higher than for the 6-fan configuration. Drag for the various arrangements of model 4 can be more accurately estimated by Eq. (2)

$$\frac{\Delta D}{T_S} = \frac{D_R}{T_S} + \frac{D_i}{T_S} = \frac{D_R}{T_S} + \left(\frac{\Delta L_i}{T_S}\right)^2 \frac{T_S}{2\rho A_m V^2} \qquad (2)$$

where the last term is induced drag based on lift on the wing, and the momentum area (A_m) defined by the lifting element span. This use of the induced drag relationship can be justified because the major portion of the induced lift is concentrated near the fans. If the full wing span momentum area is used, the induced drag change with number of spanwise fans is quite small.

3.1.5 Pitching moment.- Turning of airflow into the fan causes a nose-up pitching moment as airspeed is increased. Fig. 18 shows the variation of moment, normalized by lift and effective fan diameter, with flight speed ratio for several configurations. The tandem fan arrangement of model 6 shows the smallest variation of moment with airspeed. When trailing-edge flaps are used, the curve for nose-down pitching moment from the flap tends to level off, then go in an increasing nose-down direction as airspeed is increased. Thus a trailing-edge flap usually reduces moments required for trim. The slope of this curve in the low-speed region can be used as an indicator of moment variation with airspeed, and has been presented as a function of local diameter to chord ratio (8). More recent results have been added to that data and are shown in Fig. 19. Except for the tandem fan arrangement (model 6a), the slope of the curve increases as diameter to local chord ratio decreases. As with induced lift, chordwise placement of the fans causes significant variations of moment with airspeed. Although there are some exceptions, the results indicate high induced lift will usually generate large moments.

Since these moments appear as forces on the wing, it should be possible to calculate the moment from the induced lift equation. If the center of lift on the areas fore and aft of the fan is assumed to fall at one-half of their respective chords, the equation for

center-of-pressure location in fractions of fan radius is

$$\frac{a}{R} = \frac{\frac{\Delta L_{i_1}}{T_s}\left(\frac{x}{R} + 2\right) + \frac{\Delta L_{i_3}}{T_s}\left(1 + \frac{C}{R} - \frac{x}{R}\right)}{2\left(\frac{T}{T_s} + \frac{L_{i_1}}{T_s} - \frac{L_{i_3}}{T_s}\right)} \qquad (3)$$

A comparison of experimental and calculated center of pressure movement is given below:

Model	$\partial(a/R)/\partial(V_o/V_j)$ Experimental	$\partial(a/R)/\partial(V_o/V_j)$ Calculated	Agreement between experimental and theoretical induced lift
1	3.5	1.6	Poor
2	3.4	4.2	Good
3	3.9	2.7	Poor
4a	7.2	7.3	Good
4b	7.0	8.4	Fair
4c	8.4	9.2	Fair
4d	5.2	8.4	Good
5	4.7	4.3	Poor
6a	2.9	2.5	Good
6b	5.7	8.8	Good
6c	5.4	20.2	Poor

The table shows that center-of-pressure movement was predicted reasonably well 7 times out of 11, the same ratio as for induced lift, but good agreement with induced lift did not always produce good agreement for moment.

3.1.6 Effect of fan operation on flap effectiveness.- The effect of fan operation on the aerodynamic contributions of a trailing-edge flap is shown for model 4 in Figs. 20 to 22. Model 4 had a full-span single-slotted trailing-edge flap. Fig. 20 shows the effect of fan operation on flap lift increment as a function of flight velocity ratio. Fig. 21 shows the effect of fan operation on drag increment, and Fig. 22 shows the effect on moment increment. These figures indicate that fan operation did affect these flap increments, especially when six fans were operating. The amount and direction of the fan effects varied greatly with number of fans, velocity ratio, and exit louver deflection and whether fans were fore or aft in the wing. These large effects of fan operation on flap increments are not clearly understood. The peculiarities of flow in this area should be studied carefully to assure obtaining the maximum benefits from flaps.

3.2 Performance

3.2.1 Ground effect.- Fig. 23 shows the variation of lift and thrust with ground height for models 1 and 3. Fan thrust decreased with height at constant rpm nearly the same amount for both the wing and fuselage installation. Most of the thrust loss occurred below 2 diameters, and was caused by reduced airflow in the region of the hub. The thrust loss would be smaller if constant power operation were permissible. For model 1, with the single fan, the total lift loss at 1 diameter was quite severe, about 2/3 was caused by the thrust loss and about 1/3 by adverse interactions between the ground and the model. For model 3, with two fans, favorable interactions with the ground cancelled the fan thrust loss, so that total forces on the model did not vary with ground height.

Ground effect on model 4 with 6 fans operating is shown in Fig. 24. Here, the distance to the ground is measured from the bottom of the fuselage; the average fan height is about 2 diameters higher. In this case, fan thrust was constant, because of the high wing installation. The lift loss in ground effect was about 3 percent, but the wheel fairings on the side of the fuselage caused an overall thrust loss of about 4 percent and had about the same ground effect.

3.2.2 Transition performance.- Fig. 25 shows, for model 4a, an estimate of the variation with flight speed of required thrust-to-weight ratio, exit louver deflection, and nose-mounted trim thrust required for a 6^{o} climb angle. The basic data were modified by making fan thrust variation with speed more representative of typical fan-in-wing performance. It is assumed the aircraft is designed for VTOL but can be overloaded for STOL. Results are presented for three different types of longitudinal control system. One system has no direct thrust longitudinal control system, so is limited to STOL operation by the designed unbalance of the model. The second system (called a separate control system) has an auxiliary turbojet for trim, and the third is a power transfer system that provides constant power input regardless of trim requirements. This means that all ducting is interconnected so that the power not used for trim can be absorbed by the lift fans. The separate control system shows no reduction of the required thrust-to-weight ratio until an airspeed of 70 knots is reached. In fact, because of the nose-up tendency with speed of lift-fan aircraft, the nose thrust is reduced continually to trim the aircraft as airspeed is increased from hover, but the excess installed thrust is not usable for improving STOL performance. Therefore, the aircraft cannot be loaded above the VTOL weight unless the runway is long enough to allow acceleration above 70 knots. With the aerodynamic or the power transfer control system, the thrust required at 70 knots is 80 to 82 percent of the VTOL thrust. These two control systems provide better STOL performance than the separate control system because the installed power can always be used to propel the aircraft. For an aircraft that is designed for STOL only, required thrust-to-weight ratio will be less than for the corresponding

VTOL aircraft for all three control systems. With a power transfer system, a fan rpm margin of 17 percent above the hover rpm is required. The rpm margin designed into the fans for hover control would probably suffice. At an airspeed of 50 knots, thrust-to-weight ratio required for a 6° climb is less than 0.9, and take-off distance would be about 1000 feet. This 10 percent overload capability could provide a 60 percent increase in payload capability or about a 60 percent increase in range for a lift-fan powered transport aircraft (9).

For model 7, the variation of required thrust, cruise fan duct incidence angle, exit louver deflection angle, and horizontal-tail incidence angle and angle of attack for trim are shown as a function of airspeed in Fig. 26 for a transition at 0° angle of attack. The thrust required data indicate that lift was not reduced with airspeed for this design. Duct inlet stall did not appear to be a problem for this configuration. The tail angle of attack for trim varied from 12° at 60 knots airspeed to 7° at 175 knots airspeed; this variation is not extreme, and the magnitudes are small enough that tail stall would not be a problem. About half the tail moment capability is available for maneuvering or providing stability. Even less trim would be required of the tail with a hover control contribution to trim.

3.3 Lift Fan Installation

3.3.1 Boundary-layer control.- Model 5 had a 5-percent-thick triangular wing. In order to reduce fan depth for installation of the XV-5A type fan in this thin wing, it was necessary to remove the exit stator and the outboard portion of the fan front frame and inlet. The outer 180° of the inlet was replaced by a circumferential slot which supplied a jet of high velocity air over a small radius (less than an inch in some places) defined by the available wing thickness. Over the inboard 180°, the wing was thick enough for the normal XV-5A type inlet.

Fig. 27 shows the zero airspeed performance of this fan with the BLC slot inlet with and without BLC and with and without the stator The lift fan without the stator but with BLC had more lift than the conventional fan-in-wing lift-fan installation (with the stator). With the stator on, lift was higher than that measured with a cruise fan inlet (10), and was, in fact, the highest lift ever measured for this type of fan. Fig. 28 shows the radial variation of dynamic pressure at the fan exit with and without BLC. On the side of the fan where performance was dependent on BLC, the BLC provided large gains. The other side of the fan, however, also showed a significant improvement when BLC was applied. Thus, BLC on only half the fan circumference improved flow through the whole fan. Fig. 29 shows the boundary-layer control requirements. The ratio of lift to lift without boundary-layer control is shown as a function of the ratio of BLC momentum to fan momentum. For 3 percent BLC thrust, fan thrust was increased 30 percent.

The effectiveness of boundary-layer control at forward speed is shown in Fig. 30. Thrust at forward speed was somewhat higher than with a conventional lift fan. Fig. 31 shows the variation of the ratio of lift to lift without BLC as a function of BLC to fan momentum ratio and the inverse of the flight speed ratio. This parameter is actually the ratio of BLC momentum to ram drag. Data at different fan rpm and airspeeds are correlated reasonably well by this parameter.

3.3.2 Thin fan designs.- The NASA contracted with the General Electric Company (11) to study the design of thin, high-pressure-ratio fans. Depth was minimized by providing minimum distance between components, minimum thickness stages, eliminating components, and by replacing the stator with inlet guide vanes. It was found that the latter approach improved fan thrust-to-weight ratio and lift-to-volume ratio, but slightly increased fan diameter. In Fig. 32, a 1.21 pressure ratio inlet guide vane fan is compared with the modified 1.1 pressure ratio XV-5A fan with the BLC inlet. Except for the hub, the fans have the same thickness; thus either inlet guide vane fans or BLC inlets or a combination of both can be used for very thin installations.

4. CONCLUDING REMARKS

It has been shown that interference effects, that is, lift, drag, and moment, due to lift-fan operation are large and very dependent on wing geometry, location of fans, and distribution of fans. In some cases it is possible to predict these effects. However, wing flows behind the fan are not well understood, and must be before interference effects can be calculated with confidence. Aerodynamic contributions of trailing-edge flaps may be reduced by fan operation, and research is required to define the type and location of flap that will be useful both with the fans on and off. Downwash from fans or vertically thrusting engines placed upstream of the wing will unload the wing. Induced effects on the remote fan fairings can overcome the unloading from the downwash. The flow fields from the remote lifting elements will probably interact and make estimation of total interference effects difficult.

As in other vertical jet types, ground effects on lift-fan powered aircraft are dependent on configuration. The fans themselves can be another source of lift loss in ground effect. Thrust required and moments for trim in transition are reasonable. STOL operation of overloaded VTOL lift-fan aircraft provides significant gains in range or payload.

Blowing boundary-layer control applied to very short lift-fan inlets will probably improve net performance and permit very thin, efficient, lift-fan installations. Substituting inlet guide vanes for the stator on a conventional fan may be another way of providing thin lift-fan installations.

5. REFERENCES

1. Aoyagi, Kiyoshi; Hickey, David H.; and deSavigny, Richard A.: "Aerodynamic Characteristics of a Large-Scale Model With a High Disk-Loading Fan Mounted in the Fuselage." NASA TN D-775, 1961.

2. deSavigny, Richard A.; and Hickey, David H.: "Aerodynamic Characteristics in Ground Effect of a Large-Scale Model With a High Disk-Loading Lifting Fan Mounted in the Fuselage." NASA TN D-1557, 1963.

3. Hickey, David H.; and Hall, Leo P.: "Aerodynamic Characteristics of a Large-Scale Model With Two High Disk-Loading Fans Mounted in the Wing." NASA TN D-1650, 1963.

4. Kirk, Jerry V.; Hickey, David H.; and Hall, Leo P.: "Aerodynamic Characteristics of a Full-Scale Fan-In-Wing Model Including Results in Ground Effects With Nose-Fan Pitch Control." NASA TN D-2368, 1964.

5. Hall, Leo P.; Hickey, David H.; and Kirk, Jerry V.: "Aerodynamic Characteristics of a Large-Scale V/STOL Transport Model With Lift and Lift-Cruise Fans." NASA TN D-4092, 1967.

6. Hickey, David H.; Kirk, Jerry V.; and Hall, Leo P.: "Aerodynamic Characteristics of a V/STOL Transport Model With Lift and Lift-Cruise Fan Power Plants." NASA SP-116, Paper No. 7, April 4-5, 1966.

7. Cook, Woodrow L.; and Hickey, David H.: "Comparison of Wind-Tunnel and Flight-Test Aerodynamic Data in the Transition-Flight Speed Range for Five V/STOL Aircraft." NASA SP-116, Paper No. 26, April 4-5, 1966.

8. Goldsmith, Robert H.; and Hickey, David H.: "Characteristics of Lifting-Fan V/STOL Aircraft." Astronautics and Aerospace Engineering, Oct. 1963.

9. Fry, Bernard L.: "Feasibility of V/STOL Concepts for Short-Haul Transport Aircraft." NASA CR 743, 1967.

10. Giulianetti, Demo J.; Biggers, James C.; and Corsiglia, Victor R.: "Wind-Tunnel Test of a Full-Scale, 1.1 Pressure Ratio, Ducted Lift-Cruise Fan." NASA TN D-2498, 1964.

11. Przedpelski, Zygmunt J.: "Lift Fan Technology Studies." NASA CR-761, 1967.

NOMENCLATURE

A_f	fan area, sq ft
a	distance from fan axes to center of pressure, ft
BLC	blowing boundary-layer control
b	half-span of wing, ft
C	local wing chord, ft
$C_{L_{\delta_1}}$	the variation of lift coefficient with flap deflection for unity flap-wing-chord ratio, per radian
C_T	thrust coefficient, $\frac{T}{qS}$
C_μ	momentum coefficient, $\frac{T}{qS_1}$
c	two-dimensional wing chord, ft
$\frac{C_l}{\delta_j}$	the variation of two-dimensional lift coefficient with jet momentum coefficient, per radian, $3.0\sqrt{C_\mu}$
D	fan diameter, ft
D_e	effective fan diameter, $\left(\frac{4A_f}{\pi}\right)^{1/2}$, ft
D_i	induced drag, lb
D_R	ram drag, lb
h	height from ground plane, ft
i_D	angle of incidence of rotating cruise fan ducts, deg
i_t	incidence of the horizontal tail, deg
L	lift of the model, lb
L_w	wing lift, lb
M	pitching moment, ft-lb
q	dynamic pressure, lb/ft^2
R	fan radius, ft
r	radial distance from fan axis, ft

rpm	fan rotational speed, revolutions per minute
S	wing area, sq ft
T	fan or engine gross thrust in the vertical direction, lb
V	airspeed, knots
V_j	airspeed of fan exhaust, knots
W	aircraft gross weight, lb
x	distance from leading edge of wing to fan radius, ft
α	angle of attack, deg
β	angle of exit louvers from the vertical, deg
ΔC_D	difference in drag coefficient increment due to trailing-edge flaps
ΔC_L	difference in lift coefficient increment due to trailing-edge flaps
ΔC_m	difference in pitching-moment coefficient due to trailing-edge flaps
ΔD	drag due to lift-fan operation, lb
ΔL_i	lift induced by lift-fan operation, lb
δ_j	two-dimensional jet flap angle, $\frac{90 - \beta}{57.3}$, radians
δ_n	angle of lift-cruise engine nozzles from the vertical, deg

Subscripts

FO	fan power off
s	V = 0
1,2,3	pertaining to the areas in Fig. 7
2d	two dimensional

Table 1

LARGE-SCALE MODEL GEOMETRY

MODEL	TYPE		WING ASPECT RATIO	SWEEP OF QUARTER CHORD LINE	TAPER	A_f/S	D_f/b	D_f/c	t/c	REFERENCE
1	FAN IN FUSELAGE		4	0°	1	.054	.442	.137	.24	1,2
2	FAN IN WING		3.5	0°	1	.099	.429	.269	.352	3
3	FAN IN WING		3.11	40°/25°	.42	.147	.44	.369	.43	4
4	[illegible]		3.43	25°	.47	[illegible]	[illegible]	[illegible]	[illegible]	[illegible]
5	FAN IN WING		2.9	52.4°	0	.12	.334	.161	.43	
6	[illegible]		[illegible]	35°	1	.013 .035 .035	.196 .333 .333	.164 .164 .164	.226 .226 .226	5,6
7	FOLDING LIFT FAN, ROTATING CRUISE FAN		5.8	35°	1	.123	—	—	—	5,6

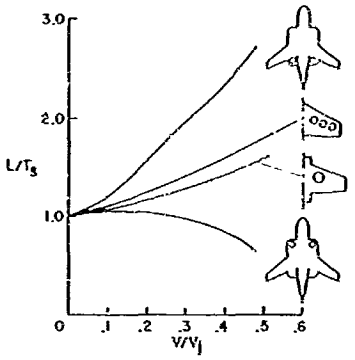

Fig. 3.- Variation of lift with airspeed for several fan-in-wing models; flaps up, $\alpha = 0^{\circ}$, $\beta = 0^{\circ}$.

Fig. 1.- Lift-fan models as mounted in the Ames Research Center 40- by 80-Foot Wind Tunnel.

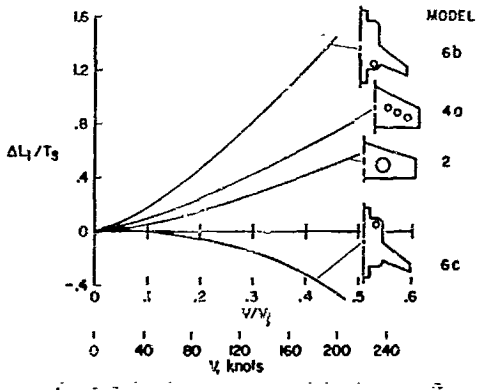

Fig. 4.- Induced lift with different lift-fan arrangements; $\delta_f = 0^{\circ}$, $\beta = 0^{\circ}$.

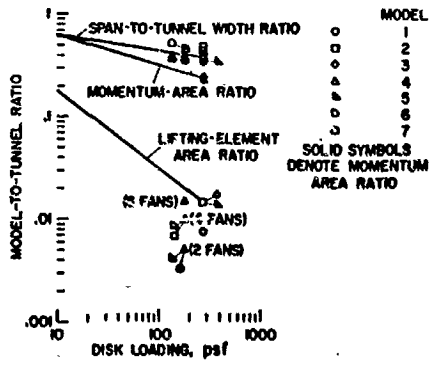

Fig. 2.- Model - wind-tunnel sizing in relation to recommended boundaries.

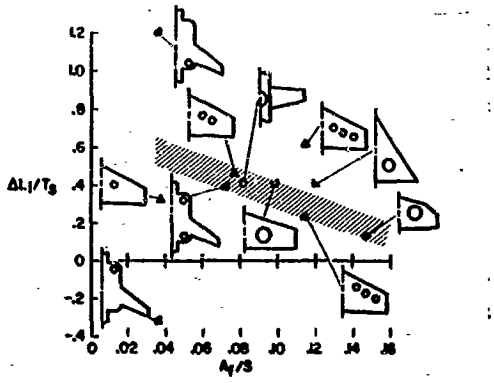

Fig. 5.- Influence of fan area to wing area ratio on induced lift; $V/V_j = 0.4$, flaps up, $\beta = 0^{\circ}$.

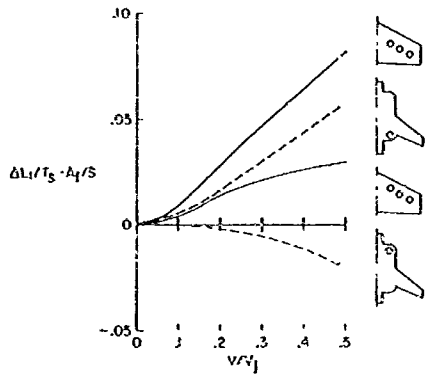

Fig. 6.- Influence of fan chordwise position on induced lift; flaps up, $\beta = 0^o$.

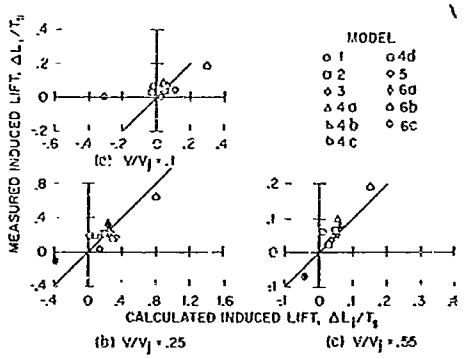

Fig. 9.- Comparison of measured and calculated induced lift for several velocity ratios; flaps up, $\beta = 0^o$.

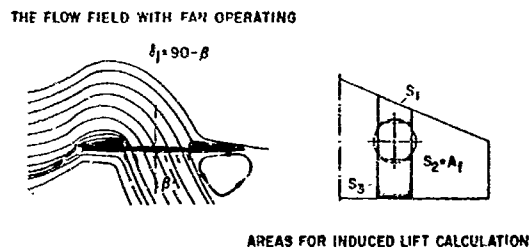

Fig. 7.- Definition of flow field and terms used for induced lift computation.

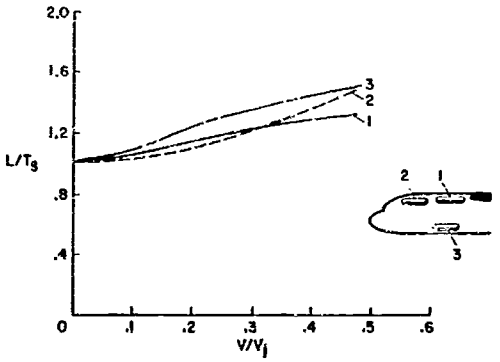

Fig. 10.- Effect of front fan location on the variation of lift with airspeed; front fans only, $\alpha = 0^o$, $\beta = 0^o$, flaps up.

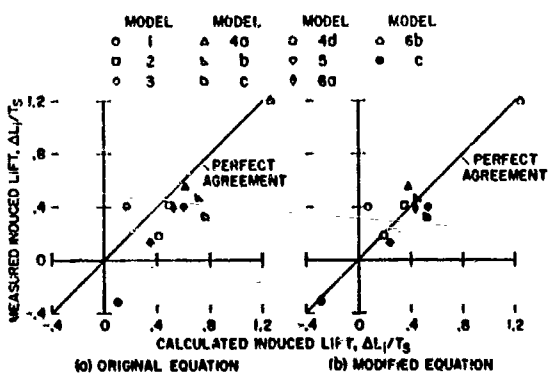

Fig. 8.- Comparison of experiment and theory; $V/V_j = 0.4$, flaps up, $\beta = 0^o$.

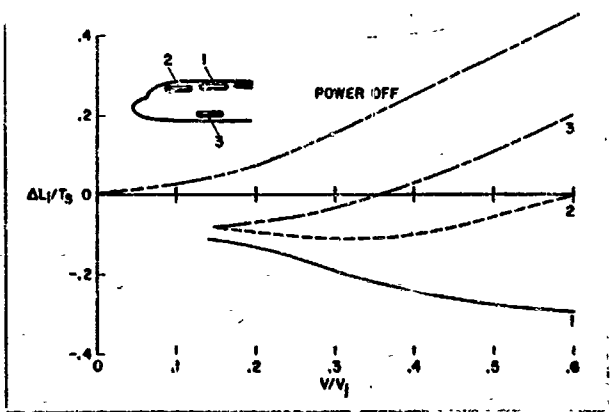

Fig. 11.- The effect of front fan operation on wing lift; flaps up, $\beta = 0^o$, $\alpha = 0^o$.

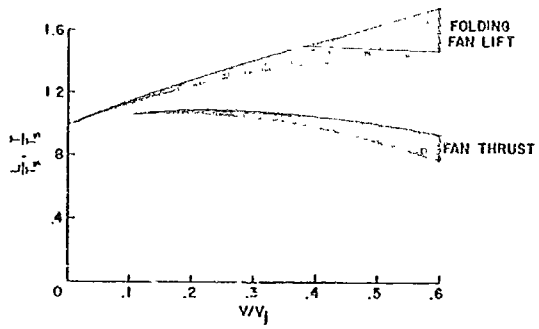

Fig. 12.- Variation of front fan lift with forward speed; $\alpha = 0^\circ$, $\beta = 0^\circ$.

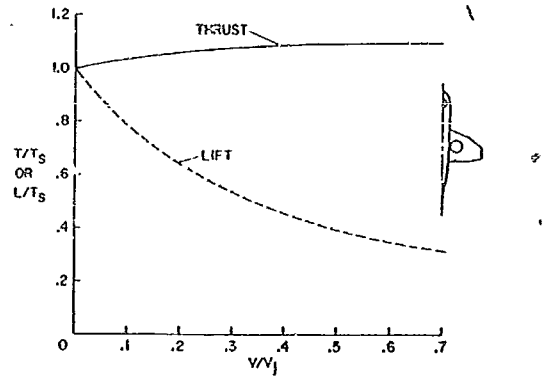

Fig. 15.- Lift contribution of a nose fan.

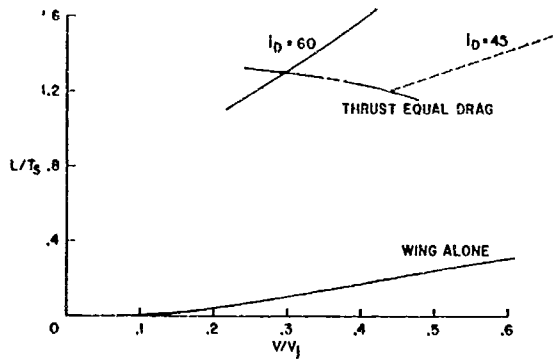

Fig. 13.- Variation with forward speed of lift of the individual components of the lift-cruise fan configuration; $\alpha = 0^\circ$.

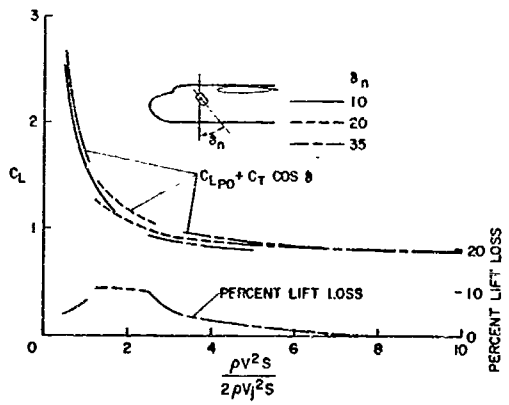

Fig. 16.- Lift loss from operation of vectored lift-cruise engines operating ahead of the wing; model 4, $\delta_f = 40^\circ$.

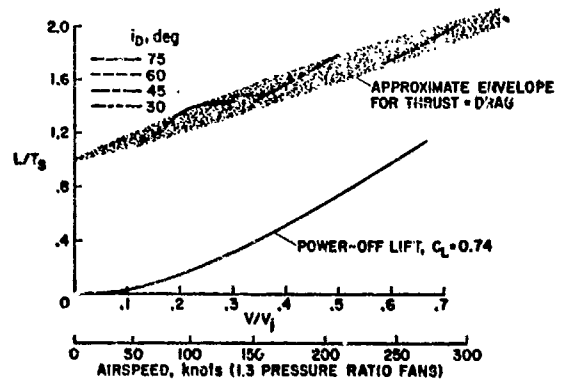

Fig. 14.- Variation of lift with airspeed; lift-cruise fan model, thrust equal drag, $\alpha = 0^\circ$, $\delta_f = 45^\circ$.

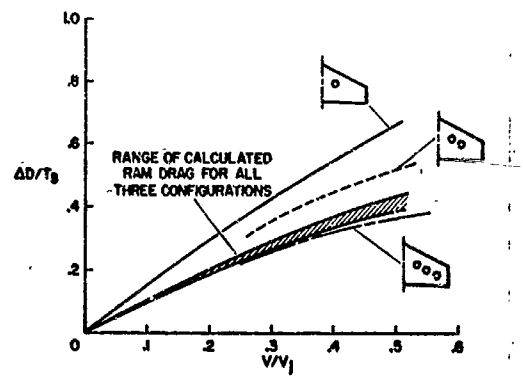

Fig. 17.- Effect of spanwise fan distribution on drag due to fan operation; $\alpha = 0^\circ$, $\beta = 0^\circ$.

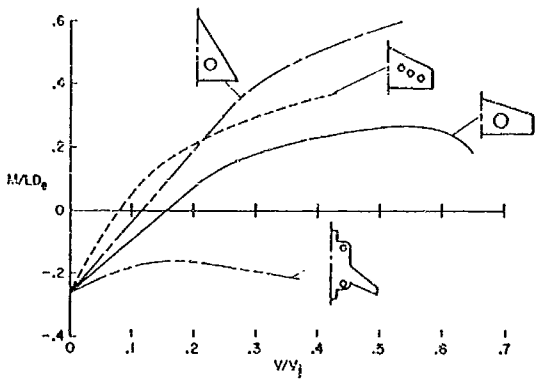

Fig. 18.- Variation of moment with airspeed; flaps up, $\alpha = 0^o$, $\beta = 0^o$.

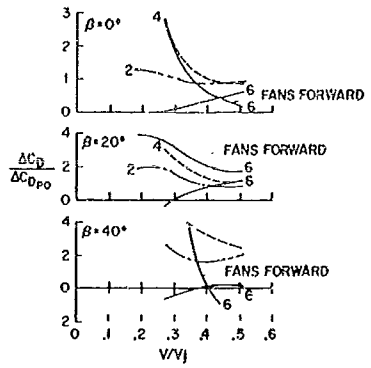

Fig. 21.- Drag due to a trailing-edge flap; model 4, $\delta_f = 40^o$.

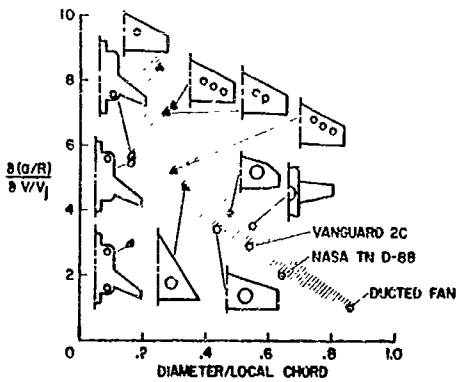

Fig. 19.- The variation of center-of-pressure shift with velocity ratio; $\alpha = 0^o$, $\beta = 0^o$.

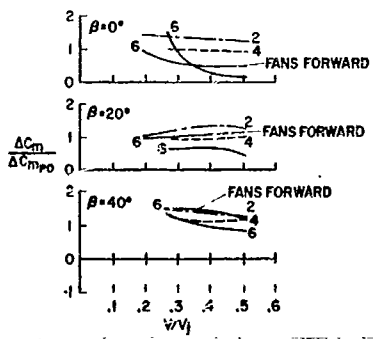

Fig. 22.- Pitching-moment contribution due to trailing-edge flaps; model 4, $\delta_f = 40^o$.

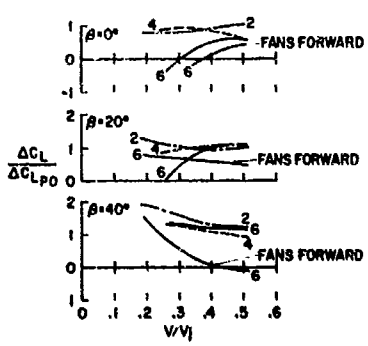

Fig. 20.- Flap effectiveness with lift fans operating; model 4, $\delta_f = 40^o$, full span.

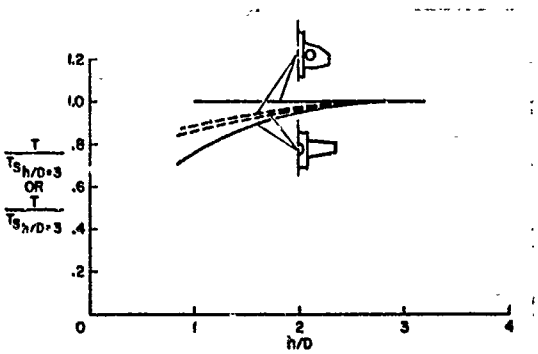

Fig. 23.- Variation of lift with distance from ground; models 1 and 3, V = 0, $\alpha = 0^o$, $\beta = 0^o$.

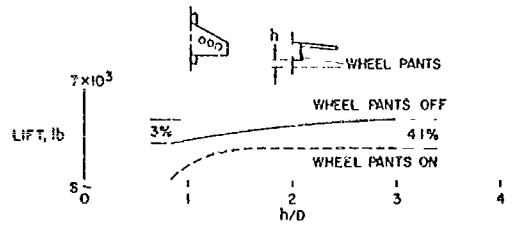

Fig. 24.- Variation of lift with model height; model 4, V = 0, $\alpha = 0^{\circ}$, $\beta = 0^{\circ}$.

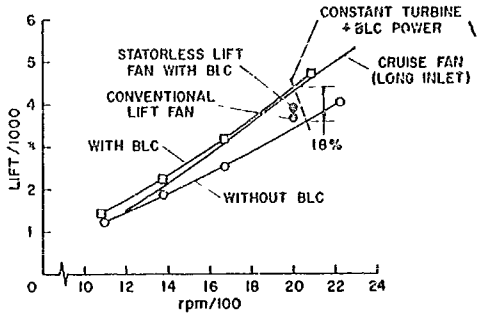

Fig. 27.- Effect of boundary-layer control; single fan, V = 0.

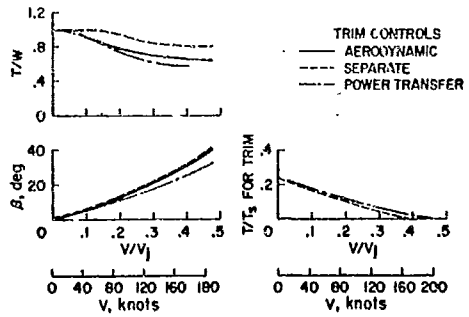

Fig. 25.- Transition performance with different control systems; 6° climb angle, $\delta_f = 40^{\circ}$, $\alpha = 0^{\circ}$.

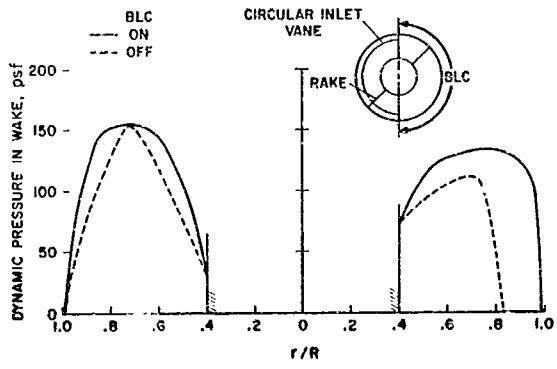

Fig. 28.- Effect of BLC on dynamic pressure in fan wake; V = 0.

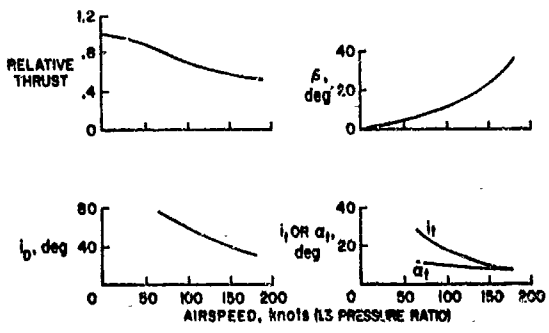

Fig. 26.- Transition characteristics of lift-cruise fan.

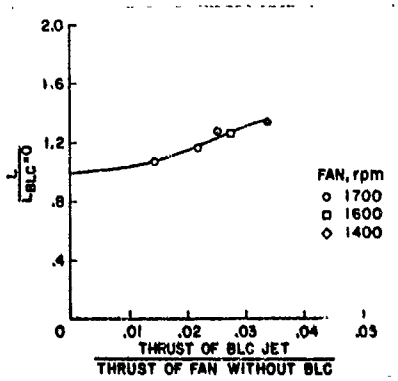

Fig. 29.- Correlation of BLC requirements; V = 0.

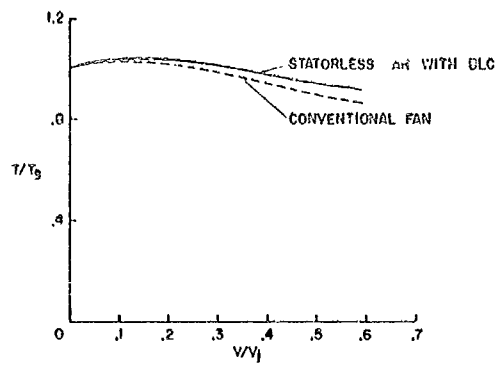

Fig. 30.- Comparison of performance of conventional fan and statorless BLC fan; $\beta = 0^{\circ}$.

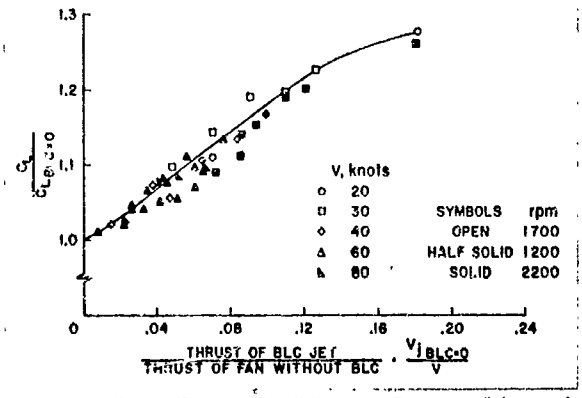

Fig. 31.- Correlation of results at several airspeeds; $\beta = 0^{\circ}$, 1700 rpm.

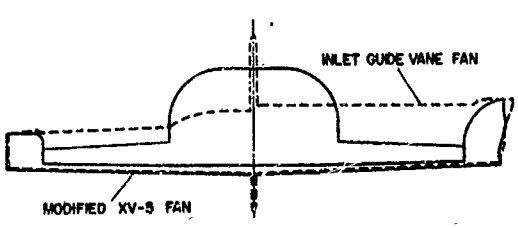

Fig. 32.- Comparison of the modified XV-5A fan with a fan with inlet guide vanes.